


Article

A Spatial 4-DOF Laser Collimation Measurement System

Han Jiang ¹, Ke Zhang ^{1,*}, Lufeng Ji ², Ruiyu Zhang ³ and Changpei Han ^{2,*} 

¹ School of Mechanical Engineering, Shanghai Institute of Technology, Shanghai 201418, China; jhtomas@163.com

² Shanghai Institute of Technical Physics, Chinese Academy of Sciences, Shanghai 200083, China; jlfouc@163.com

³ School of Cyber Science and Engineering, Wuhan University, Wuhan 430072, China; ruiyuzhang953@gmail.com

* Correspondence: zkwy2004@126.com (K.Z.); changpei_han@mail.sitp.ac.cn (C.H.)

Abstract: A compact and miniaturized laser collimation system was proposed to measure the four-degrees-of-freedom of an optical payload in high-altitude space. Compared with other systems, this system has a simple structure and low cost, high measurement accuracy, and a large measurement range. The optical structure of the system was designed, the measurement principle of the four-degree-of-freedom was described in detail, the interference between the distance measurement and the angle measurement in the optical path was analyzed, and the installation error was analyzed. The error was minimized under different temperature conditions to improve the robustness of the system. An engineering prototype was built based on the system design scheme and an experiment was conducted to measure a target with a measured distance of 500 mm. The current indicators reached the requirements for the ground testing of optical payloads. The application of the system can be used to measure six degrees of freedom simultaneously by installing two systems in different coordinate systems. The system can also be used in industry; for example, by measuring the machine tool error in real time and compensating for it, the system can improve the positioning and motion accuracy. It can also be used for feedback control of the robot's motion by measuring and controlling it.

Keywords: 4-DOF; laser collimation; space optical loading



Citation: Jiang, H.; Zhang, K.; Ji, L.; Zhang, R.; Han, C. A Spatial 4-DOF Laser Collimation Measurement System. *Appl. Sci.* **2024**, *14*, 10491. <https://doi.org/10.3390/app142210491>

Academic Editor: Douglas O'Shaughnessy

Received: 24 October 2024
Revised: 31 October 2024
Accepted: 7 November 2024
Published: 14 November 2024



Copyright: © 2024 by the authors. Licensee MDPI, Basel, Switzerland. This article is an open access article distributed under the terms and conditions of the Creative Commons Attribution (CC BY) license (<https://creativecommons.org/licenses/by/4.0/>).

1. Introduction

Spatial freedom refers to the change in straightness in the XYZ triaxial direction of an object and the change in the XYZ triaxial angle direction. Detecting the precision of spatial freedom has always been an important subject in the field of industry and aviation. Errors in machine tools in the industrial field directly affect the machining accuracy of the machine tools. The positioning and motion accuracy can be improved by measuring and compensating for machine errors in real time. In the field of industrial robots, it is necessary to detect the position of the robot, provide feedback, and control its movement. The degree of freedom of the optical electron microscope needs to be tested in real time, so it can be adjusted. In the field of aviation, with the continuous development of satellite technology in China, indicators such as the detection range, resolution, and stability of optical remote sensing satellites are increasing [1,2]. Due to the very complex carrying and operating environment of space loads, they are mainly subjected to space thermal deformation (STD) caused by the changes in solar incidence angle during launch. After these influences, the geometric positioning of the high orbit will gradually change. By affecting the relative pose between the primary mirror and the sub-mirror of the optical load, while causing the optical load to defocus, the resolution and other parameters of the optical load will be affected, and the final positioning accuracy of the camera will be affected [3–7]. Recently, a method was proposed where the freedom from the star sensor to the star is known and the freedom from the star to the ground is known, and only the freedom from the star

sensor to the optical load needs to be measured, as the freedom from the optical load to the ground can be obtained by solving this. Therefore, it is necessary to develop a system for measuring the freedom of optical load in space.

The number of degrees of freedom in a measurement can be divided into contact and non-contact types. In most scenarios in the industrial and aviation fields, where direct contact with the measured object is not possible, non-contact measurement is preferred. The current mainstream non-contact measurement method, used domestically and abroad, is to use a laser as the measurement medium. The current mainstream laser measurement methods are the interference method, diffraction method, and collimation method.

Laser interferometry has a measurement range from micrometers to meters or larger, with a measurement accuracy at the nanometer level, and its advantages include medium economic efficiency and general environmental requirements. Its advantage is its high precision, but its disadvantage is its high sensitivity to the environment, including environmental factors such as temperature, vibration, and air flow [8–11]. The advantage of using diffraction-precision microns are that they can be used for high-resolution image analysis, and are suitable for high-resolution image analysis and for observing fine structures, while their disadvantages are that they are highly demanding on the optical system and limited by the diffraction limit [12–15]. The accuracy of the collimation method is at the micron level, and its advantages are that it is simple and easy to use, has low equipment maintenance costs and a fast measurement speed, and can provide measurements over a large range. The disadvantages are affected by the stability of the light source. In summary, after comprehensively considering the accuracy and environmental economy, the optical collimation method was selected [16–19]. This is shown in Table 1.

Table 1. Optical measurement method performance comparison.

Method	Accurate	Vantage	Drawbacks	Costs	Measurement Stability
interferences	nanoscale	High precision	High environmental sensitivity to environmental conditions such as temperature, vibration and air movement	High	If the optics have a small amount of displacement, distortion, or surface quality, this can affect the formation and stabilization of the interference fringes. In addition, temperature and air pressure can also affect the results.
diffraction	Micron-scale	Can be used for high-resolution image analysis; suitable for high-resolution image analysis; suitable for observation of fine structures	High demands on the optical system; limited by diffraction limits	High	The wavelength of the light source, the quality of the beam and the precision of the experimental setup are highly required. If these conditions are not met, the quality of the diffraction pattern will be affected.
collimation	Micron-scale	Simple to use; low equipment maintenance; fast measurement speeds over a wide area	Affected by light source stability	Low	When the environmental factors (temperature, humidity, vibration, etc.) are better controlled, the stability is higher. The use of certain techniques and equipment, such as single-mode optical fiber, can effectively reduce the impact of temperature drift and obtain more stable results in a shorter period of time

Li Ze of Dalian University of Technology developed a 5-DOF geometric error measurement system for machine tool tables based on interferometry, which is used to determine the error correction accuracy of machine tool errors in the range $\pm 1 \mu\text{m}$, angle measure-

ments of ± 1 , repeatable distance measurements of $2.5 \mu\text{m}$, and angle measurements of 2.5 [20], but is easily affected by the environment. B. Chen et al. proposed a laser net difference straightness interferometer for the simultaneous measurement of 6-DOF motion errors. Multiple degrees of freedom are measured using spacing changes and counting the interference fringes. This measurement method makes full use of the high-precision characteristics of laser interferometry, but the system is complex and the cost is high [21,22]. Based on the principle of grating spectroscopy, the laser grating method achieves multi-degrees-of-freedom measurement by obtaining the different pieces of information carried by each separate beam of light. C. Lee et al. propose a 6-DOF measurement method using a single optical encoder unit and discuss uncertainty estimations in terms of error sources [9], but the system is complex and costly.

Compared with the Dalian University of Technology, Li Ze developed an interferometric method based on the machine tool table five-degrees-of-freedom geometric error measurement system. Halo is a four-quadrant detector QD. My system uses three CMOS; the impact on the CMOS image surface of the spot changes to dissolve the straightness of the moving end of the angular change to improve the measurement of the range, the X-direction range of $\pm 2.0 \text{ mm}$, Y-direction range of $\pm 1.6 \text{ mm}$, X-direction pitch angle range of $\pm 1.9^\circ$, and Y-direction yaw angle range of $\pm 1.4^\circ$. The range of X-direction is $\pm 2.0 \text{ mm}$, the Y-direction range is $\pm 1.6 \text{ mm}$, the X-direction pitch angle range is $\pm 1.9^\circ$, and the Y-direction yaw angle range is $\pm 1.4^\circ$. Compared with B. Chen et al., who proposed a laser net straightness interferometer for the simultaneous measurement of six-degrees-of-freedom motion errors, my system has a simpler structure and the laser collimation method is less affected by different environments, such as high temperatures. The method also adapts better to low altitudes, vacuum, and other conditions. The cost of my system is lower compared to the six-degrees-of-freedom measurement method using a single optical encoder unit proposed by C. Lee et al.

The reason that a multi-DOF measurement system is developed in this paper is that it is necessary to measure multiple DOFs simultaneously in real time in order to adjust the DOF of the optical load in high space and solve the defocusing phenomenon. Therefore, it is necessary to develop a multi-DOF measurement system. Six-degrees-of-freedom systems contain some principle problems: a set of systems are required to measure six degrees of freedom at the same time, and the Z-axis requires the interference method to be used, while the Z-axis roll angle measurement requires a high-precision method; these problems should be further studied [23–25]. The actual measurements of six degrees of freedom can be made using two systems: one system placed as shown in the figure and the other with the laser output light perpendicular to the YOZ plane of the optical load.

The measurement principle of the optical system developed in this paper uses the optical collimation method. The principle of the optical collimation method is that the laser has directivity and the exit angle is approximately 0° , which can be regarded as parallel light. When reflecting from a plane, parallel light changes slightly when the plane is moved in a certain direction of freedom. The principle of laser optical collimation range and angle measurement can be used to calculate the value of displacement or the angle according to the slight change in the displacement of parallel light and the relationship between displacement and distance or angle.

Section 2 of the article describes the basic principle of the optical path structure and separately describes the ranging optical path, angle measurement optical path, optical isolator's basic principle, and the measurement results of the optical path diagram principle crosstalk analysis.

Section 3 of the article continues the error analysis to the CMOS installation error, using the homogeneous transformation matrix method for the analysis.

In Section 4, the system is built according to the schematic diagram of the optical path, the change in the small degree of freedom of the mobile terminal is simulated, the system is measured, and the calibration test and stability test are carried out.

Section 5 of the article describes the technical route of the paper, clearly showing the steps from the beginning of the research to the system's development and testing.

Section 6 of the article describes the conclusion of the paper, summarizes the article, and describes the technical specifications of the system.

2. Optical Principle

As mentioned earlier, the laser collimation method was used for the design. The principal diagram of the four-degree-of-freedom measurement system is shown in Figure 1. Since the laser diode is small in size and has a long life, it is suitable for high-altitude space environments; therefore, the laser diode was used. Since the actual laser will have a divergence angle, it is necessary to use a collimator to convert it to parallel light to improve the performance and accuracy of the optical system. Two corner cone prisms were used: one was the integrated angle measurement and ranging of the light path, while the other was used to eliminate the effect of the pitch angle and yaw angle on the straightness measurements and reduce the influence of crosstalk. These will be described in detail in Section 2.3 CMOS was used to calculate the change in the position of the moving end by measuring the moving position of the laser on the target surface; this is described in detail in Sections 2.1 and 2.2. The reason other photodetectors were not used is that, with a four-quadrant detector, the angle measurement range is not large enough; therefore, small CCD or CMOS photodetectors should be used. Compared with CCD, CMOS has lower power consumption and can achieve a faster image reading rate. The polarization beam splitter (PBS2) and the quarter wave plate QWP were combined to form the optical isolator. The light intensity regulator was composed of a half-wave plate HWP and polarization beam-splitter (PBS1). Other optical lenses, such as spectroscope BS2, were used to change the light path, so that the ideas discussed in Sections 2.1 and 2.2 could be realized; otherwise, the laser would be covered and could not reach the CMOS.

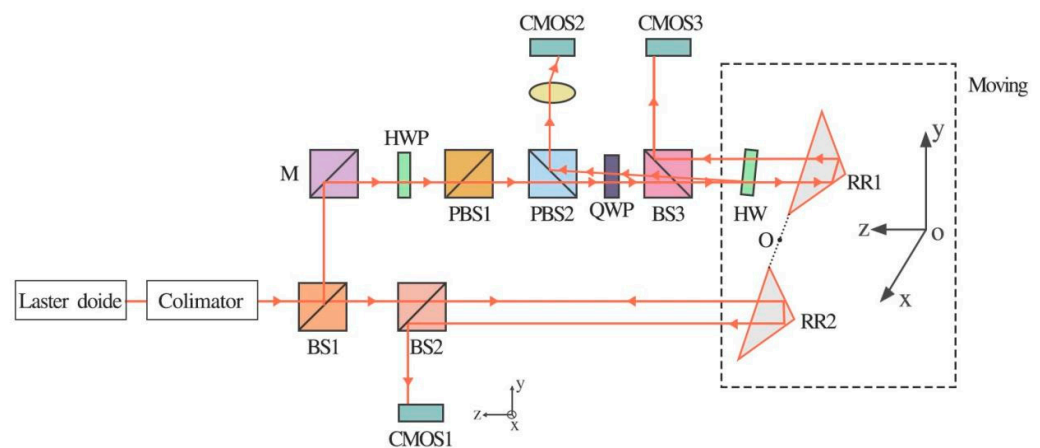


Figure 1. Optical schematic diagram of the system.

2.1. Ranging Optical Path

As shown in Figure 2, the laser diode emits laser light, which becomes collimated after collimation by the collimator. A beam is reflected by the beam-splitter (BS1), which hits the plane mirror (M), is reflected by the plane mirror (M), and passes through the half-wave plate HWP, the polarization beam-splitter (PBS1), PBS2, the quarter-wave plate (QWP), the beam-splitter (BS3), the semi-transparent and semi-reflective mirror HW, and the corner cone prism (RR1). After being reflected by RR1, it hits the beam splitter (BS3), is reflected by BS3, and then hits the image plane of CMOS3. When the corner cone prism RR1 moves, the light spot on the image plane of CMOS3 moves; this light path was used to measure the displacement in the x/y direction.

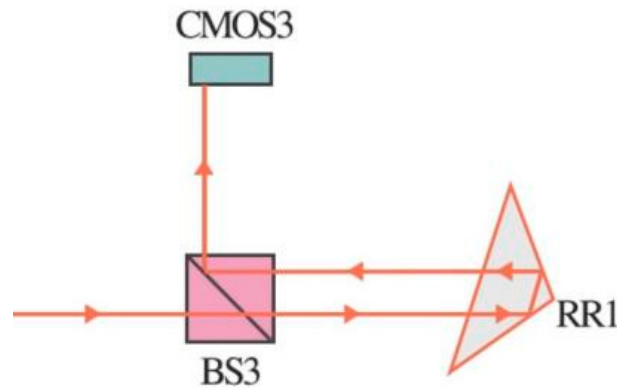


Figure 2. X/Y direction straightness ranging optical path.

As shown in Figure 3, another beam is passed through the beam-splitter (BS1 and BS2), hits the corner cone prism RR2, and is reflected by the corner cone prism (RR2), before returning, hitting the beam-splitter (BS2), being reflected by BS2, and hitting the CMOS1 image plane. When angular cone prism RR2 moves, the light spot on the image plane of CMOS1 moves, and this light path is used to measure the displacement in the x/y direction (Figure 4).

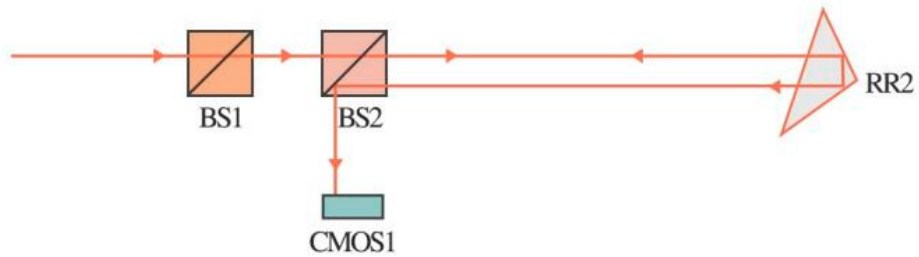


Figure 3. X/Y direction ranging optical path.

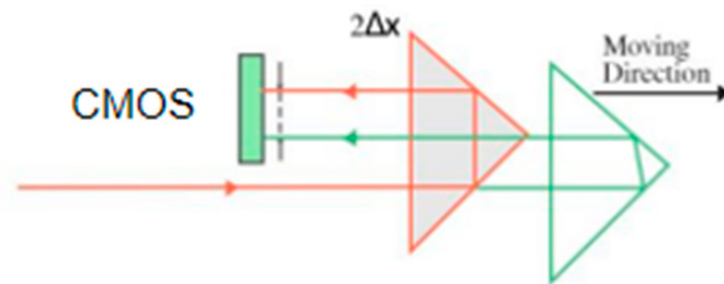


Figure 4. Principal diagram of ranging light path.

When the angle cone prism moves up and down or left and right, it will cause a change in the incident point, which will lead to a corresponding relative displacement between the outgoing beam, that is, a change in the position in which the detector receives the light. According to the formula, when the angular cone prism is moved x distance, $2x$ displacement will occur between the outgoing light and the original outgoing light. The four-quadrant detector will convert the change in spot position into a change in the current through photoelectric conversion, and the displacement value can be obtained after signal processing and calibration.

$$\Delta_X = \frac{\Delta_{CMOS}}{2} \tag{1}$$

$$\Delta_Y = \frac{\Delta_{CMOS}}{2} \tag{2}$$

In sum, as long as the deviation of the laser beam in the x/y direction on the four-quadrant detector CMOS Δ_{CMOS} is obtained, a change in the straightness of Δ_X and Δ_Y in the x/y direction can be obtained.

2.2. Angle-Measuring Optical Path

As shown in Figure 5, another beam is reflected by beam-splitter BS1 and hits plane mirror M. After being reflected by plane mirror M, it passes through the polarizing beam-splitter (PBS1, PBS2), quarter-wave plate (QWP), beam-splitter (BS3), and half-transparent half-reflective mirror HW, which is reflected by HW, before hitting the polarizing beam-splitter (PBS2), where it is reflected and hits the CMOS2 image plane. When the half-transparent half-reflective mirror HW moves, the spot on the CMOS2 image plane moves, and this optical path is used to measure changes in the x/y direction angle, i.e., the pitch and roll angles.

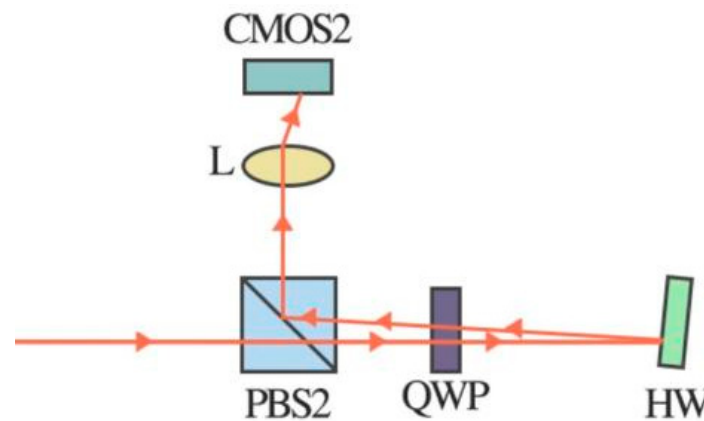


Figure 5. The pitch angle in the X direction and yaw angle in the Y direction, which are used to measure the optical path.

After the light source is collimated by the collimating mirror, it forms a parallel beam of light, which then becomes incident on the polarization beam-splitter, where the polarization state is separated. The transmitted light is P-polarized, while the reflected light is S-polarized. When the P-polarized light beam center is perpendicularly incident on the center of the semi-transparent half-reflective mirror, the outgoing light travels in the opposite direction to the incident light and is separated by the polarization beam splitter to achieve signal isolation. Then, it is focused by the convex lens to the center of the focal plane. If the semi-transparent half-reflective mirror undergoes a small angle of bending α , the reflected light will bend by 2α degrees, and the parallel light will be focused by the lens and converge on the focal plane. Finally, by calculating the change in the focus position of the image plane, the angle change can be characterized.

As shown in Figure 6, when the target object moves, the angular cone prism RR moves accordingly, and the angular deflection angle and pitch angle of the angular cone prism in the x/y direction shift α and β , respectively. The beam is refracted through the plano convex lens L, and the angle between the beam and the central horizontal axis of the plano convex lens L is 2α or 2β . A laser is irradiated on the surface of the CMOS light-sensitive material and is received by it, with an offset of x . The beam forms a triangle with the central horizontal axis and the line on the focal plane of the plano-convex lens L, which can be determined using the following equation:

$$x = f \tan 2\alpha \quad (3)$$

$$y = f \tan 2\beta \quad (4)$$

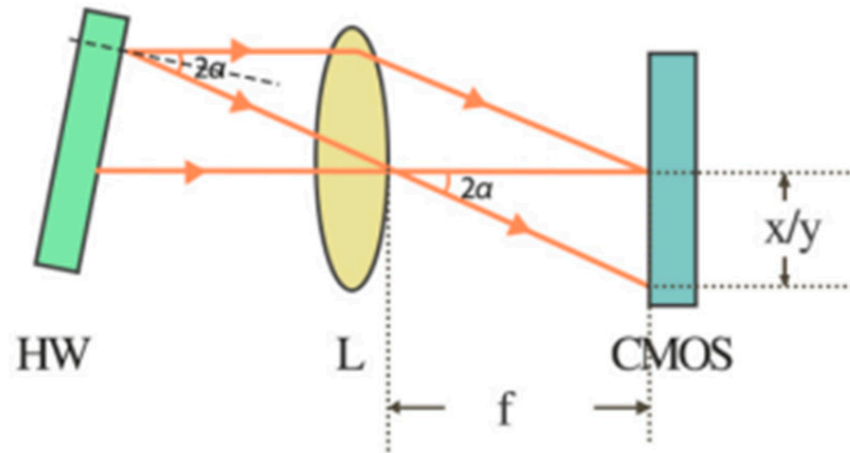


Figure 6. Principal diagram of angle measurement light path.

When the alpha and beta are small, the following equation can be used:

$$\tan 2\alpha \approx 2\alpha \quad (5)$$

$$\tan 2\beta \approx 2\beta \quad (6)$$

Then,

$$\alpha = \frac{x}{2f} \quad (7)$$

$$\beta = \frac{y}{2f} \quad (8)$$

In sum, as long as the offset of the laser beam on the CMOS is obtained, it can be divided by the focal length f of the flat convex lens L twice to find the deflection angle α and pitch angle β .

2.3. Crosstalk Analysis of Measurement Results

2.3.1. Using Two CMOS Detectors for Ranging and Angle Measurement Crosstalk Analysis

The spot displacement x and y , received by the detector measuring displacement, are determined using the outgoing beam of the corner cone prism. According to the characteristics of the corner cone prism, the position and angle of the incident beam affect the position of the outgoing beam. Linear displacement Z and rolling angle do not affect the incident light spot of the angle cone prism, while the pitch angle and yaw angle will affect the incident light spot of the angle cone prism beam. The use of two CMOS detectors can eliminate the influence of the angle of deflection and pitch angle on the range of x/y direction straightness. A more detailed analysis is provided as follows.

Analysis of Crosstalk of Angle Measurement and Range Using the Traditional Geometric Method

The influence of pitch angle and deflection angle measurements on horizontal ranging: When the corner cone prism is rotated around an edge angle of O , take RR2 as an example for analysis, Hypothesis: Deflection angle α will only cause measurement errors in the x direction range; deflection angle β will only cause error in the y direction range.

Figure 7 is the coordinate system, the angle in the x direction is the pitch angle (yaw), and the angle in the y direction is the deflection angle (pitch).

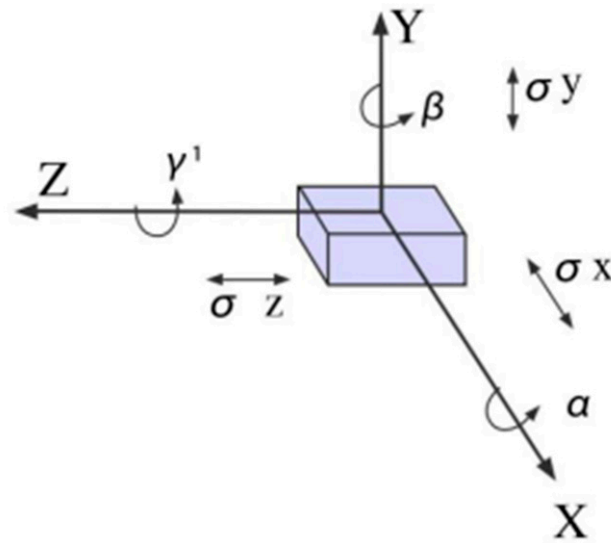


Figure 7. System coordinates.

As shown in Figure 8, assume the ideal case first. The errors of the pitch angle and deflection angle are α and β respectively, when the cone prism RR rotates around the edge of angle O, which is the ideal case, and when the right angle radius of the cone prism is r , as shown in this figure. It can be seen that the influence of the two laser beams I1 and I2 in the x direction is twice as large as the deviation of the projection in the x direction of the center P and the P' of the right angle radius of RR and RR' figures before and after the corner prism δ_x .

$$\delta_x = 2r(1 - \cos \alpha) \tag{9}$$

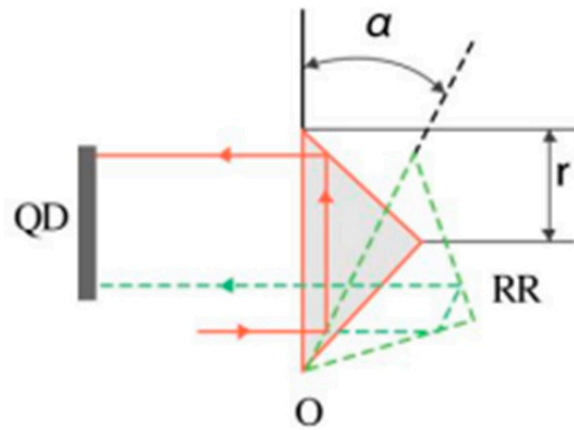


Figure 8. The angular cone prism, rotated around edge angle O.

Similarly, the influence in the y direction of by deflection angle β is δ_y

$$\delta_y = 2r(1 - \cos \beta) \tag{10}$$

The corner cone prism is rotated around the non-edge O point (Figure 9).

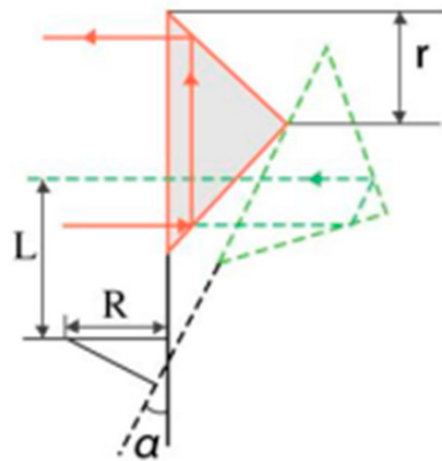


Figure 9. The corner cone prism rotates around the non-edge O point.

Further considering the actual situation, assuming that RR1 and RR2 rotate around O, as shown in the figure. In the actual model, the angular prism rotates around the non-edge O point. δ_x , which is the deviation of laser beams I1 and I2, is still twice as large as the influence of the deviation of the center P and the P' of the right-angle radius of the RR and RR' figures at the front and back of the angular prism in the x direction, in addition to S. The projected distance from the lower edge point of the corner cone prism to the rotation point O in the x direction is L, the vertical distance from the rotation point O to the right angle side of RR is R, and S is twice as big as the projection of L on the right angle side of RR'; that is, S is $2R\sin\alpha$:

$$\delta_{x1} = 2[(r + R)(1 - \cos \alpha) + L \sin \alpha] \tag{11}$$

Similarly, the influence of deviation in the y direction caused by deflection angle β is δ_y :

$$\delta_{y1} = 2[(r + R)(1 - \cos \beta) + L \sin \beta] \tag{12}$$

The pitch angle α and the deflection angle β are around 200, so $\cos\alpha$ and $\cos\beta$ are approximately 1; therefore, the sum can be simplified to δ_x and δ_y :

$$\delta'_{x1} = 2L \sin \alpha \tag{13}$$

$$\delta'_{y1} = 2L \sin \beta \tag{14}$$

As the angular cone prism will double the straightness ranging result, the actual result is δ_x and δ_y :

$$\delta''_{x1} = L \sin \alpha \tag{15}$$

$$\delta''_{y1} = L \sin \beta \tag{16}$$

As the light is on the lower half of RR1, and the light on RR2 is on the upper half, the influence of pitch angle on the straightness range is the opposite to that of the deflection angle, which is δ_x and δ_y . The conclusion of RR1 is as follows:

$$\delta''_{x2} = -L \sin \alpha \tag{17}$$

$$\delta''_{y2} = -L \sin \beta \tag{18}$$

Therefore, as long as the position changes in CMOS1 and CMOS2, which are the ranging results, are added, the joint effects of deflection angle and pitch angle can be eliminated.

$$\Delta_X = \frac{\Delta_{\text{CMOS1}} + \Delta_{\text{CMOS3}}}{4} \tag{19}$$

$$\Delta_Y = \frac{\Delta_{CMOS1} + \Delta_{CMOS3}}{4} \tag{20}$$

3. Error Analysis

3.1. Analysis of Installation Error (Abbe Error) Using the Homogeneous Transformation Matrix Method

A. The homogeneous transformation matrix method was used for the installation error (Abbe error) analysis.

The central coordinate point O0O1 of O-X1Y1Z1 should be perpendicular to the $O0 \times OY0$ and $O1X1Y1$ planes, and the axes of the moving-end coordinate system and the fixed-end coordinate system $O0-X0Y0Z0$ should be parallel to one another. However, as Figure 10 illustrates, there will be a misalignment between the fixed-end coordinate system $O0-X0Y0Z0$ and the moving-end coordinate system $O-X1Y1Z1$. This misalignment can be measured using six indicators and is referred to as an installation error (Abbe error). That is, the position error is Δ_X , Δ_Y , and Δ_Z in the three directions of the XYZ axis of the two coordinate systems; the Angle error is α , β , and γ in the three directions of the XYZ axis. This misaligned state can be represented by the homogeneous coordinate matrix H . The homogeneous matrix H contains all six of these indicators, which are Δ_X , Δ_Y , Δ_Z , α , β and γ .

$$H = \begin{bmatrix} 1 & \alpha & -\beta & \Delta_X \\ -\alpha & 1 & \gamma & \Delta_Y \\ \beta & -\gamma & 1 & \Delta_Z \\ 0 & 0 & 0 & 1 \end{bmatrix} \tag{21}$$

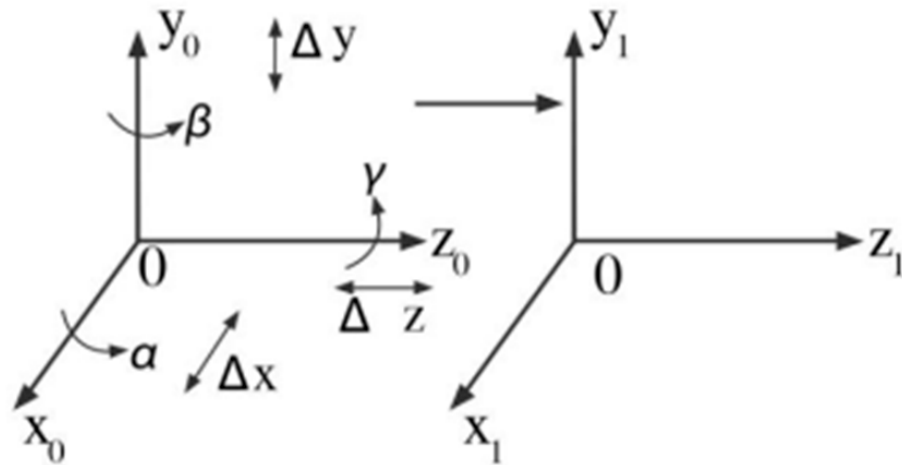


Figure 10. CMOS installation error model.

B. Establishment of a straightness error model under the homogeneous transformation matrix method.

The straightness error, which does not consider the installation error, can be represented by matrix P_{CMOS1_0} :

$$P_{CMOS1_1} = HP_{CMOS1_0} = \begin{bmatrix} 1 & \alpha & -\beta & \Delta_X \\ -\alpha & 1 & \gamma & \Delta_Y \\ \beta & -\gamma & 1 & \Delta_Z \\ 0 & 0 & 0 & 1 \end{bmatrix} [2\delta_X \quad 2\delta_Y \quad 0 \quad 1]^T = \begin{bmatrix} 2\delta_X + 2\alpha\delta_Y + \Delta_X \\ 2\delta_Y - 2\alpha\delta_X + \Delta_Y \\ 2\beta\delta_X - 2\gamma\delta_Y + \Delta_Z \\ 1 \end{bmatrix} \tag{22}$$

Therefore, the straightness error in the x direction is $2\delta_X + 2\alpha\delta_Y + \Delta_X$, and the straightness error in the y direction is $2\delta_Y - 2\alpha\delta_X + \Delta_Y$

i.e., equality:

$$\delta'_X = \delta_X + \alpha\delta_Y + \frac{\Delta_X}{2} \tag{23}$$

$$\delta'_Y = \delta_Y - \alpha\delta_X + \frac{\Delta_Y}{2} \tag{24}$$

$\frac{\Delta_X}{2} / \frac{\Delta_Y}{2}$ represents the translation errors due to CMOS1 installation, which have the same effect on each measuring point. This effect can be eliminated using differential operations between the measuring point and the initial point. $\alpha\delta_X / \alpha\delta_Y$ is the straightness distance crosstalk between two straightness errors; α can be determined via calibration. δ_X / δ_Y is the original ideal straightness distance in the X and Y directions.

C. Establishment of the error model of pitch angle and deflection angle under the homogeneous transformation matrix method.

The direction vector of the laser beam in the O0-X0Y0Z0 coordinate system and the direction vector after being reflected by plane mirror M can be represented as follows:

$$\vec{n} = [0 \ 0 \ 1] \vec{n}_1 = [2\alpha \ 2\beta \ -1] \tag{25}$$

As shown in Figure 11, according to the ABCD matrix, in the coordinate system O0-X0Y0Z0, in the X-axis direction, the laser beam matrix that considers the distance to the planar convex lens can be expressed as $L M_X$:

$$M_X = \begin{bmatrix} 1 & L \\ 0 & 1 \end{bmatrix} \begin{bmatrix} 0 \\ 2\alpha \end{bmatrix} = \begin{bmatrix} 2L\alpha \\ 2\alpha \end{bmatrix} \tag{26}$$

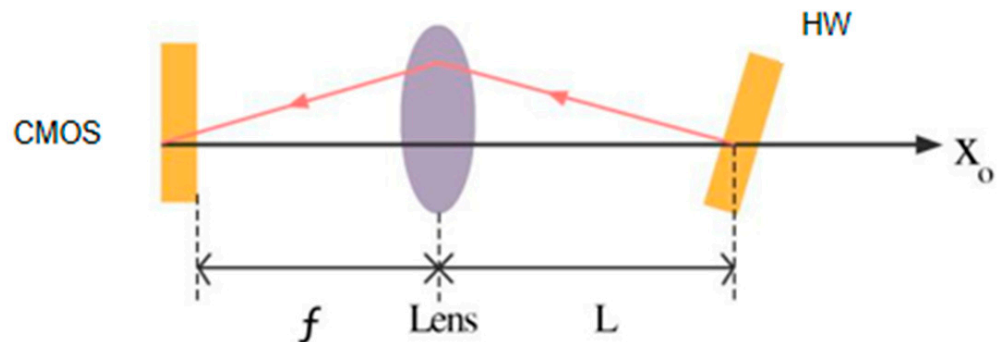


Figure 11. Influence of CMOS translation installation error on the X-axis.

In the coordinate system O0-X0Y0Z0, in the Y-axis direction, the laser beam matrix that considers the distance to the planar convex lens can be expressed as $L M_Y$:

$$M_Y = \begin{bmatrix} 1 & L \\ 0 & 1 \end{bmatrix} \begin{bmatrix} 0 \\ 2\beta \end{bmatrix} = \begin{bmatrix} 2L\beta \\ 2\beta \end{bmatrix} \tag{27}$$

For L , after the distance, the offset distance of the laser beam in the X-axis direction is $2L\alpha$ and the angle offset is 2α , while the offset distance in the Y-axis direction is $2L\beta$ and the angle offset is 2β .

As shown in the figure, when using plane convex lens L , the laser beam matrix in the X direction can be expressed as follows:

$$M_{X1} = \begin{bmatrix} 1 & 0 \\ -f & 1 \end{bmatrix} \begin{bmatrix} 2L\alpha \\ 2\alpha \end{bmatrix} = \begin{bmatrix} 2L\alpha \\ 2(1 - Lf)\alpha \end{bmatrix} \tag{28}$$

As shown in the figure, after passing through planar convex lens L, the laser beam matrix in the Y direction can be expressed as follows:

$$M_{Y1} = \begin{bmatrix} 1 & 0 \\ -f & 1 \end{bmatrix} \begin{bmatrix} 2L\beta \\ 2\beta \end{bmatrix} = \begin{bmatrix} 2L\beta \\ 2(1-Lf)\beta \end{bmatrix} \tag{29}$$

For L, after the distance and after the plane convex lens L refraction, the offset distance of the laser beam in the X-axis direction is $2L\alpha$ and the angle offset is $2(1-Lf)\alpha$, while the offset distance in the Y-axis direction is $2L\beta$ and the angle offset is $2(1-Lf)\beta$.

Then, the laser beam matrix in the direction of O1-X1Y1Z1 is calculated as follows:

$$P_{CMOS2_1} = HP_{CMOS2_0} = \begin{bmatrix} 1 & \alpha & -\beta & \Delta_X \\ -\alpha & 1 & \gamma & \Delta_Y \\ \beta & -\gamma & 1 & \Delta_Z \\ 0 & 0 & 0 & 1 \end{bmatrix} \begin{bmatrix} 2L\alpha \\ 2(1-Lf)\alpha \\ 2L\beta \\ 2(1-Lf)\beta \end{bmatrix} \tag{30}$$

$$= \begin{bmatrix} 2L\alpha + 2(1-Lf)\alpha^2 - 2L\beta^2 + 2(1-Lf)\beta\Delta_X \\ -2L\alpha^2 + 2(1-Lf)\alpha + L\beta\gamma + 2(1-Lf)\beta\Delta_Y \\ 2L\alpha\beta - 2(1-Lf)\alpha\gamma + 2L\beta + 2(1-Lf)\beta\Delta_Z \\ 2(1-Lf)\beta \end{bmatrix}$$

The pitch angle error in the X direction is $2L\alpha + 2(1-Lf)\alpha^2 - 2L\beta^2 + 2(1-Lf)\beta\Delta_X$; the yaw angle error in the Y direction is $-2L\alpha^2 + 2(1-Lf)\alpha + L\beta\gamma + 2(1-Lf)\beta\Delta_Y$

$$\alpha' = 2L\alpha + 2(1-Lf)\alpha^2 - 2L\beta^2 + 2(1-Lf)\beta\Delta_X \tag{31}$$

$$\beta' = -2L\alpha^2 + 2(1-Lf)\alpha + L\beta\gamma + 2(1-Lf)\beta\Delta_Y \tag{32}$$

Due to the complexity of error compensation after error analysis, this paper is limited in terms of space and cannot go into detail. The relevant content regarding error compensation will not be discussed in future work.

3.2. BP Neural Network Error Compensation Model

3.2.1. BP Neural Working Principle

As shown in the Figure 12, X is the input signal of the BP neural network and W is the weight parameter from the input layer to the hidden layer. Each input signal corresponds to a weight parameter, and the input signal and the weight parameter are multiplied in pairs then summed together. The threshold value is compared with the calculated cumulative sum; if it is greater, then the output signal O_j is generated by the activation function f. On the contrary, the neuron does not generate an output signal.

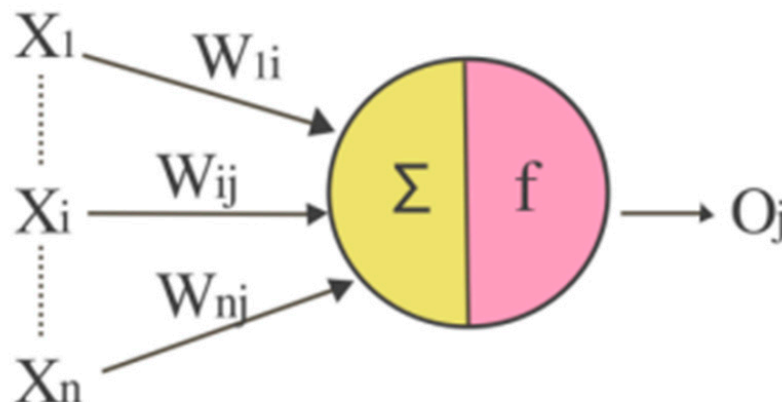


Figure 12. Neuronal structural model.

3.2.2. Error Compensation Model Based on BP Neural Network

The approximation object of the neural network model used in this section is the straightness and angle at 20 °C, i.e., the values of the six mounting error indicators, which are corrected to 20 °C at different temperatures, while the inputs are the values of the original temperature and the mounting error indicators, i.e., the schematic diagram of the neural network model shown in the Figure 13. The neural network model contains two input nodes; T is the original temperature; $\Delta_x/\Delta_y/\Delta_z/\alpha/\beta/\gamma$ represent the mounting error indicators; $\Delta'_x/\Delta'_y/\Delta'_z/\alpha'/\beta'/\gamma'$ represent the training collected from the full-temperature experiment; $\Delta''_x/\Delta''_y/\Delta''_z/\alpha''/\beta''/\gamma''$ represent the prediction sample.

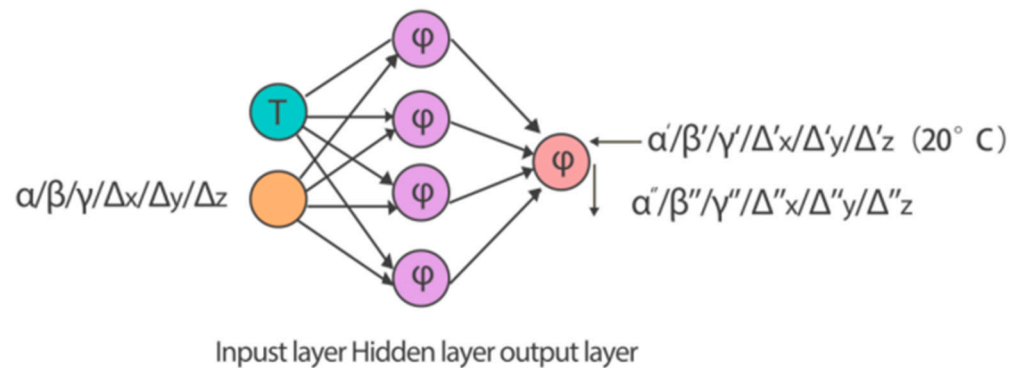


Figure 13. BP neural network temperature compensation model’s structure.

MATLAB R2022a toolbox processing was used to obtain six indicators of the temperature change and to predict the difference, followed by compensation. The six indicators were no longer affected by temperature; the base value was basically maintained at 20 °C for the calibration factor and the fluctuations showed a bias value of zero. Therefore, the stability of the output was greatly improved.

4. Experiment and Results

To verify the reliability and validity of the method, an experimental setup was established according to the schematic diagram shown in Figure 1, as shown in Figure 14. CMOS uses Hikvision’s MV-CS050-10GM with a resolution of 2048 × 2448, an imaging area of 8.8 mm × 6.6 mm (H × V), and a pixel size of 3.45 μm × 3.45 μm. The laser uses Sorebo’s LP633-SF50 with a laser center wavelength of 633 nm, the collimator uses Lubang Optoelectronics’ RFCAG-3.9-PC, and the theoretical spot diameter is 3.9 mm. The distance between the light source and the moving unit is 500 mm. Distance and focal length do not affect the measurement accuracy, only the measurement resolution. A series of experiments were carried out under laboratory conditions.

4.1. Calibration Test

According to the above measurement principles, the linear distance change and change in angle theory have a linear relationship with the measured value of the detector. Therefore, the measurement errors in the system can be obtained using a calibration test.

As shown in Figure 15, the test calibration uses the H-825 displacement platform of the PI company: the load capacity is 30 kg, the minimum moving distance and displacement are 0.1 μm, the angle is 0.0001°, the self-locking n stroke range is ± 27.5 mm, the rotation range is ±19, the n minimum incremental motion ranges up to 0.25 μm in X, Y, and Z, and n repeatability is ±0.1 μm/±2 μrad for the BLDC motor and absolute encoder.

The calibration curves of XY straightness and angle around XY are shown in Figure 16.

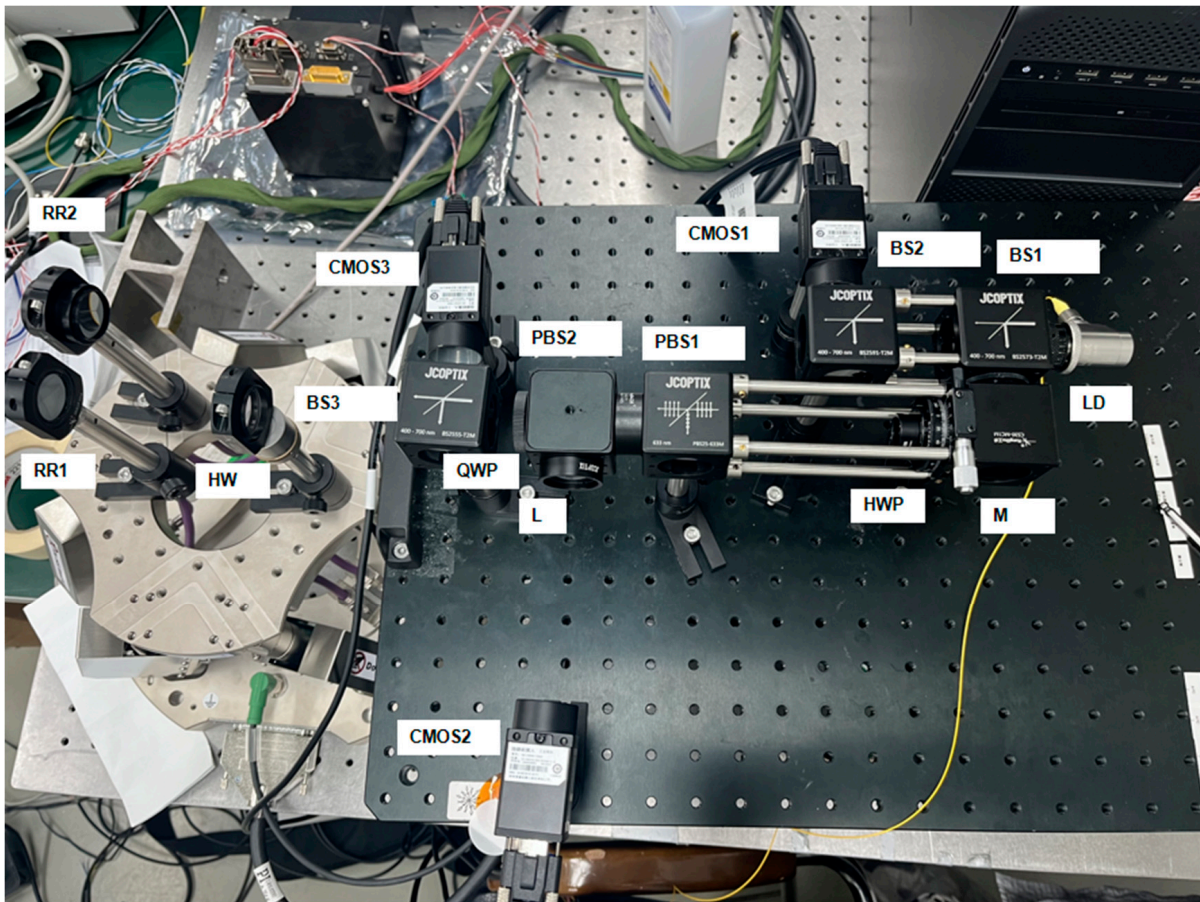
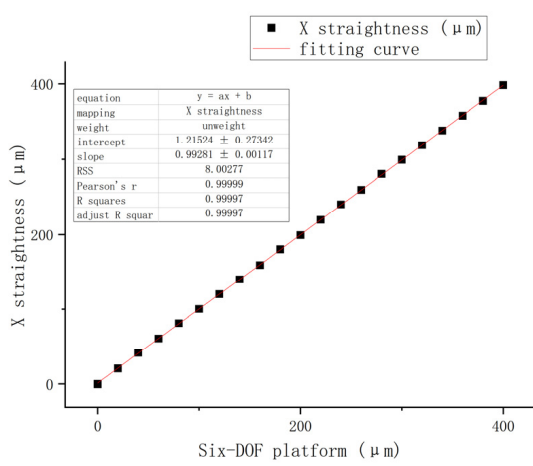


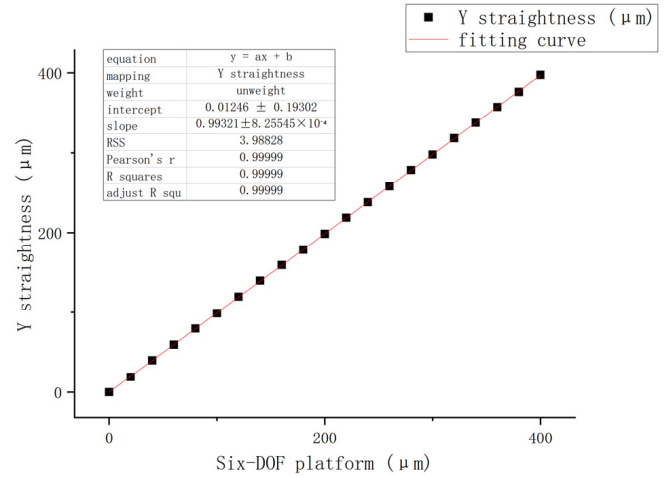
Figure 14. Four-degrees-of-freedom measuring system test device.



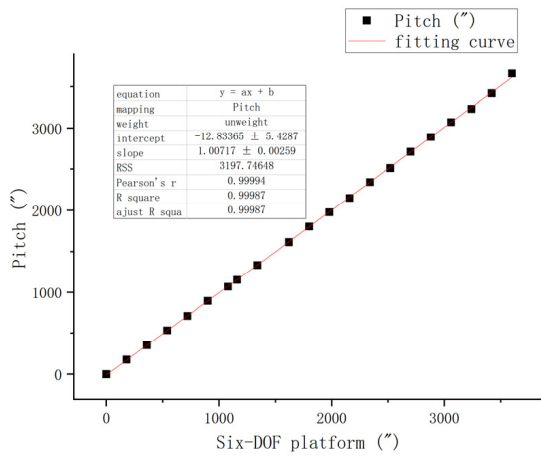
Figure 15. PI Company's H-825 displacement table.



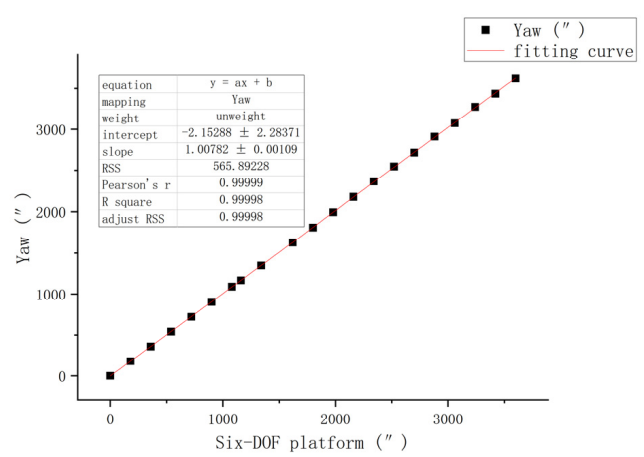
(a)



(b)



(c)



(d)

Figure 16. Calibration experiments: (a) X straightness calibration curve; (b) Y straightness calibration curve; (c) calibration curve of pitch in the X direction; (d) calibration curve of yaw in the Y direction.

4.2. Stability Test

The stability of the system was tested under laboratory conditions. The ambient temperature range at the time of measurement was 20 ± 0.5 °C. The experiment lasted for 30 min, and the data were collected every 10 s. The experimental results are shown in Figure 17. The standard deviations of horizontal and vertical straightness were $1.11 \mu\text{m}$ and $0.94 \mu\text{m}$, respectively. The standard deviations of yaw angle and pitch angle were 0.91 arcsec and 0.90 arcsec, respectively. From the above data, it can be seen that the proposed system has good stability.

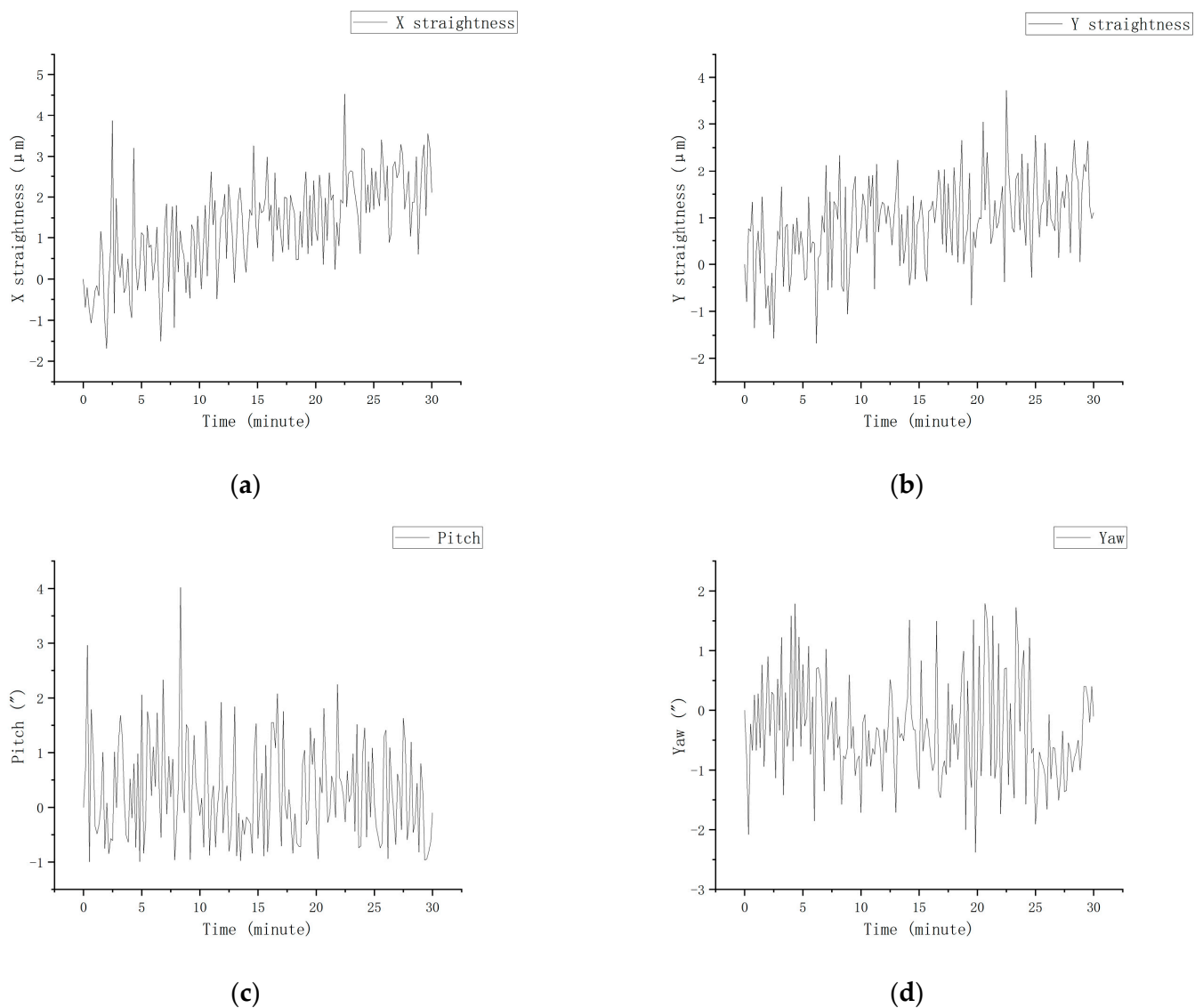


Figure 17. Results of the stability experiments: (a) X straightness SD = 1.11 μm ; (b) Y straightness; (c) pitch SD = 0.91 arcsec; (d) yaw SD = 0.90 arcsec.

5. Technical Approach in the Article

The paper first carried out a theoretical calculation of resolution and range, divided into x/y straightness and x/y direction angle to determine the optical path design and electronic circuit design, respectively. Then, the system test optical path was built, before optical path debugging was carried out, preliminary tests were conducted, and laser spot images were collected. Then, the algorithm was determined and test data were collected. Thirdly, an error analysis was conducted. Then, further calibration and stability tests were conducted, before the results were finally analyzed (Figure 18).

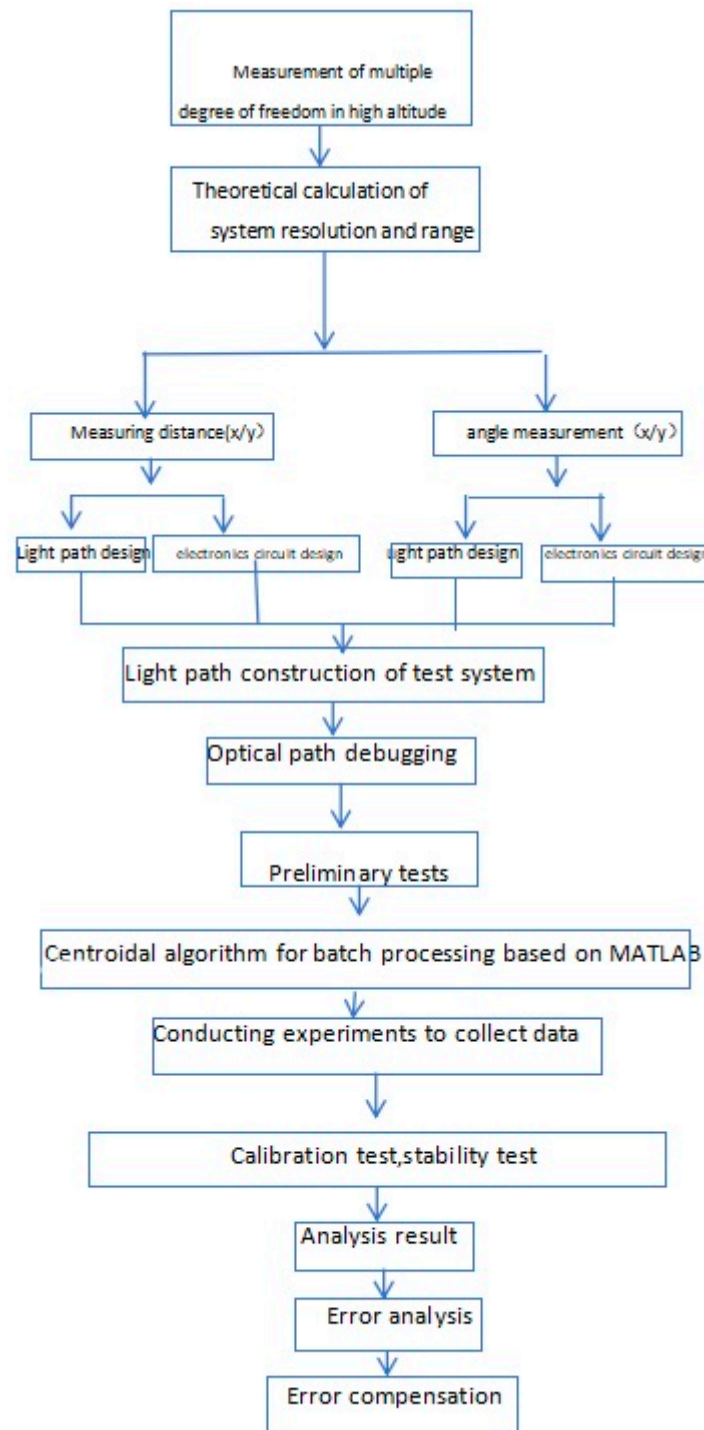


Figure 18. Article's technical route.

6. Conclusions

The 4-DOF measuring system in this paper uses the laser collimation method, which has the characteristics of miniaturization, a low cost, and high precision. Three CMOS were used, which can reduce the crosstalk caused by the results of the distance measurement and angle measurement. According to the system design scheme, an engineering prototype was built to carry out experiments with a target measured distance of 500 mm. The measuring range in the X direction was ± 2.0 mm, the measuring range in the Y direction was ± 1.6 mm, the linearity in the X direction was better than 0.99997, and the linearity in Y direction was better than 0.99999. The stability of the distance measurements in the X direction reached

1.11 μm and the stability in the Y direction reached 0.94 μm . The pitch angle measuring range in the X direction was $\pm 1.9^\circ$; the yaw angle measuring range in the Y direction was $\pm 1.4^\circ$; the linearity of the pitch angle in the X direction was better than 0.99987; the linearity of the yaw angle in the Y direction was better than 0.99998; the stability of the pitch angle in the X direction was 0.91 arcsec; the stability of the yaw angle in the Y direction was 0.90 arcsec. At present, the index meets the requirements of the optical load ground test.

The system has good reference value for machine tool precision measurements and other industrial fields, and is also suitable for high-altitude space precision measurements of optical load.

Author Contributions: Conceptualization, H.J. and L.J.; methodology, K.Z. and C.H.; software, H.J.; validation, H.J., L.J. and C.H.; formal analysis, H.J. and K.Z.; investigation, H.J. and L.J.; resources, C.H., K.Z. and L.J.; data curation, H.J.; writing—original draft preparation, H.J.; writing—review and editing, H.J., R.Z., K.Z. and C.H.; visualization, R.Z.; supervision, R.Z.; project administration, H.J. and L.J.; funding acquisition, C.H. and K.Z. All authors have read and agreed to the published version of the manuscript.

Funding: This research received no external funding.

Institutional Review Board Statement: Not applicable.

Informed Consent Statement: Not applicable.

Data Availability Statement: The original contributions presented in the study are included in the article, further inquiries can be directed to the corresponding authors.

Conflicts of Interest: The authors declare no conflicts of interest.

References

- Gao, Y.; Deng, Y.; Zhang, J. Near space optical load design key indicators and technical review. *Space Technol.* **2023**, *88*–93. (In Chinese) [[CrossRef](#)]
- Wang, F.; Zhou, F.; Zheng, G.; Zhao, H. Development of optical remote sensing payload for China Space Station. *Space Return Remote Sens.* **2010**, *31*, 27–31. (In Chinese)
- Li, X.; Yang, L.; Su, X.; Hu, Z.; Chen, F. A correction method for thermal deformation positioning error of geostationary optical payloads. *IEEE Trans. Geosci. Remote Sens.* **2019**, *57*, 7986–7994. [[CrossRef](#)]
- Huang, J.; Luo, D.; Hou, P.; You, C.; Kong, X.; Fu, X. Thermal deformation test and measurement technology of optical remote sensing satellite platform. *Spacecr. Eng.* **2018**, *27*, 114–118. (In Chinese)
- Yang, L.; Wang, Y.; Wei, L.; Hu, Z. Thermal deformation optimization of payload mounting surface of an optical satellite based on honeycomb laying technology. *Opt. Precis. Eng.* **2019**, *29*, 1043–1051. (In Chinese) [[CrossRef](#)]
- Li, X.F.; Zhang, B.L.; Lin, M. Finite element analysis of thermal deformation effect of optical mirror in space environment. *J. Optoelectron. Laser* **2005**, 906–909. (In Chinese)
- Zhu, C.; Deng, L.; Tang, Z.; Jia, J.; Wu, J.; Wang, T. Optical load Optical Axis Thermal Deformation Detection System and Method. China Patent G01M99/002, 1 December 2020.
- Auclair, P.; Bacon, D.; Baker, T.; Barreiro, T.; Bartolo, N.; Belgacem, E.; Bellomo, N.; Ben-Dayan, I.; Bertacca, D.; Besancon, M.; et al. Cosmology with the laser interferometer space antenna. *Living Rev. Relativ.* **2023**, *26*, 5.
- Lee, C.B.; Kim, G.H.; Lee, S.K. Design and construction of a single unit multi-function optical encoder for asix-degree-of-freedom motion error measurement in an ultraprecision linear stage. *Meas. Sci. Technol.* **2011**, *22*, 105901. [[CrossRef](#)]
- Yang, M.; Cai, C.; Wang, D.; Wu, Q.; Liu, Z.; Wang, Y. Symmetric differential demodulation-based heterodyne laser interferometry used for wide frequency-band vibration calibration. *IEEE Trans. Ind. Electron.* **2024**, *71*, 8129–8137. [[CrossRef](#)]
- Zhang, Y.; Guzman, F. Quasi-monolithic heterodyne laser interferometer for inertial sensing. *Opt. Lett.* **2022**, *47*, 5120–5123. [[CrossRef](#)]
- Ali, A.; Chiang, Y.W.; Santos, R.M. X-ray diffraction techniques for mineral characterization: A review for engineers of the fundamentals, applications, and research directions. *Minerals* **2022**, *12*, 205. [[CrossRef](#)]
- Tirole, R.; Vezzoli, S.; Galiffi, E.; Robertson, I.; Maurice, D.; Tilmann, B.; Maier, S.A.; Pendry, J.B.; Sapienza, R. Double-slit time diffraction at optical frequencies. *Nat. Phys.* **2023**, *19*, 999–1002. [[CrossRef](#)]
- Fatimah, S.; Ragadhita, R.; Al Husaeni, D.F.; Nandiyanto, A.B.D. How to calculate crystallite size from x-ray diffraction (XRD) using Scherrer method. *ASEAN J. Sci. Eng.* **2022**, *2*, 65–76. [[CrossRef](#)]
- Omori, N.E.; Bobitan, A.D.; Vamvakeros, A.; Beale, A.M.; Jacques, S.D.M. Recent developments in X-ray diffraction/scattering computed tomography for materials science. *Philos. Trans. R. Soc. A* **2023**, *381*, 20220350. [[CrossRef](#)]

16. Zhao, H.; Ding, W.; Fan, M.; Xia, H.; Yu, L. An optical method based auto-collimation for measuring five degrees of freedom error motions of rotary axis. *Rev. Sci. Instrum.* **2022**, *93*, 125110. [[CrossRef](#)]
17. Liu, W.; Zhang, C.; Duan, F.; Fu, X.; Bao, R.; Li, X.; Yan, M. A high-precision calibration method of PSD in long-distance laser auto-collimation system. In Proceedings of the 2021 International Conference on Optical Instruments and Technology: Optoelectronic Measurement Technology and Systems, Online, 8–10 April 2022; SPIE: Bellingham, DC, USA, 2022; Volume 12282, pp. 249–259.
18. Diao, K.; Liu, X.; Yao, Z.; Lu, W.; Yang, W. Improved calibration method of a four-quadrant detector based on Bayesian theory in a laser auto-collimation measurement system. *Appl. Opt.* **2022**, *61*, 5545–5551. [[CrossRef](#)] [[PubMed](#)]
19. Xiong, K.; He, X.; Wang, C.; Li, J.; Yang, C. Calibration method of fisheye camera for high-precision collimation measurement. *Infrared Laser Eng.* **2024**, *53*, 20230549-1–20230549-111.
20. Li, Z. Design of 5-DOF Geometric Error Measurement System for Machine Tool Table. Ph.D. Thesis, Dalian University of Technology, Dalian, China, 2019.
21. Chen, B.; Xu, B.; Yan, L.; Zhang, E.; Liu, Y. Laser straightness interferometer system with rotational error compensation and simultaneous measurement of six degrees of freedom error parameters. *Opt. Express* **2015**, *23*, 9052–9073. [[CrossRef](#)]
22. Lou, Y.; Yan, L.; Chen, B.; Zhang, S. Laser homodyne straightness interferometer with simultaneous measurement of six degrees of freedom motion errors for precision linear stage metrology. *Opt. Express* **2017**, *25*, 6805–6821. [[CrossRef](#)]
23. Zhao, Y.; Zhang, B.; Feng, Q. Measurement system and model for simultaneously measuring 6DOF geometric errors. *Opt. Express* **2017**, *25*, 20993–21007. [[CrossRef](#)]
24. Li, J.; Feng, Q.; Bao, C.; Zhang, B. Method for simultaneously and directly measuring all six-DOF motion errors of a rotary axis. *Chin. Opt. Lett.* **2019**, *17*, 011203.
25. Cui, C.; Feng, Q.; Zhang, B.; Zhao, Y. System for simultaneously measuring 6DOF geometric motion errors using a polarization maintaining fiber-coupled dual-frequency laser. *Opt. Express* **2016**, *24*, 6735–6748. [[CrossRef](#)] [[PubMed](#)]

Disclaimer/Publisher’s Note: The statements, opinions and data contained in all publications are solely those of the individual author(s) and contributor(s) and not of MDPI and/or the editor(s). MDPI and/or the editor(s) disclaim responsibility for any injury to people or property resulting from any ideas, methods, instructions or products referred to in the content.